CHEMBIOCHEM

DOI: 10.1002/cbic.200800180

An ACP Structural Switch: Conformational Differences between the Apo and Holo Forms of the Actinorhodin Polyketide Synthase Acyl Carrier Protein

Simon E. Evans,[a] Christopher Williams,[a] Christopher J. Arthur,[a] Steven G. Burston,[b] Thomas J. Simpson,[a] John Crosby,[a] and Matthew P. Crump*[a]

The actinorhodin (act) synthase acyl carrier protein (ACP) from Streptomyces coelicolor *plays a central role in polyketide biosynthesis. Polyketide intermediates are bound to the free sulfhydryl group of a phosphopantetheine arm that is covalently linked to a conserved serine residue in the holo form of the ACP. The solution NMR structures of both the apo and holo forms of the ACP are reported, which represents the first high resolution comparison of these two forms of an ACP. Ensembles of twenty apo and holo structures were calculated and yielded atomic root mean square deviations of well-ordered backbone atoms to the average coordinates of 0.37 and 0.42 Å, respectively. Three restraints defining the protein to the phosphopantetheine interface were identified. Comparison of the apo and holo forms revealed previously undetected conformational changes. Helix III moved towards helix II (contraction of the ACP), and Leu43 on helix II subtly switched from being solvent exposed to forming intramolecular interactions with the newly added phosphopantetheine side chain. Tryptophan fluorescence and* S. coelicolor *fatty acid synthase (FAS) holo-synthase (ACPS) assays indicated that apo-ACP has a twofold higher affinity (K_d of 1.1 μM) than holo-ACP (K_d of 2.1 μM) for ACPS. Site-directed mutagenesis of Leu43 and Asp62 revealed that both mutations affect binding, but have differential affects on modification by ACPS. Leu43 mutations in particular strongly modulate binding affinity for ACPS. Comparison of apo- and holo-ACP structures with known models of the* Bacillus subtilis *FAS ACP–holo-acyl carrier protein synthase (ACPS) complex suggests that conformational modulation of helix II and III between apo- and holo-ACP could play a role in dissociation of the ACP–ACPS complex.*

Introduction

Common to all fatty acid (FAS), polyketide (PKS) and nonribosomal peptide (NRPS) synthases is a remarkable component, the acyl or peptidyl carrier protein (A/PCP).[1] ACP takes the form of a small individual protein in the noncovalently associated type II synthases or a discrete folded domain when part of a multidomain type I system. It is central to all of these unique biosynthetic systems and must effectively control substrate specificity as well as mediate numerous protein–protein interactions. These include interactions with holo-acyl carrier protein synthase (ACPS), ketosynthase (KS), chain length factor (CLF) and other downstream enzymes, such as the ketoreductase (KR), aromatase (ARO) and cyclase (CYC).

The ACP family (60-100 amino acids) is characterized by a fold that consists of four α-helices (I–IV). Each carrier protein has a conserved serine residue at the N terminus of helix II. This residue is subject to post-translational modification by ACPS,[2] which transfers a 4′-phosphopantetheine (4′-PP) moiety from coenzyme A (CoA) to the serine. The activity of ACP is dependent on this conversion from the inactive apo to the active holo form. Cocrystal structures along with mutational studies have provided an excellent basis for the structural understanding of the ACP–ACPS interactions.[3–5] A comparison of the free and bound holo-ACP structures revealed a conformational change in helix II that could be important for transfer of the 4′-PP from CoA.[6] Dissociation of the complex might be assisted by relaxation of the bound (holo) form to the free holo form. The apo and holo forms of ACP were reported to be almost identical, and this similarity is supported by evidence from several structural studies. NMR spectroscopy studies on the solution structures of a number of ACPs showed no significant differences in chemical shift between apo and holo forms, and no NOEs were detected between the 4′-PP side chain and the protein. Transient interactions with the protein have been reported, though these have been assumed not to significantly alter its structure.[7–9] In the case of malarial parasite *Plasmodium falciparum* holo-ACP (PfACP), however, NOEs were observed between the protein (residues Ser37, Leu38 and Asp39) and the 4′-PP side chain. No comparison was made, however, with the apo form.[10]

Despite attracting much attention, there are no directly comparable high quality apo and holo structures for the same

[a] *Dr. S. E. Evans, Dr. C. Williams, Dr. C. J. Arthur, Prof. T. J. Simpson, Dr. J. Crosby, Dr. M. P. Crump*
School of Chemistry, University of Bristol
Cantock's Close, Bristol, BS8 1TS (UK)
Fax: (+44) 117-9298611
E-mail: matt.crump@bristol.ac.uk

[b] *Dr. S. G. Burston*
Department of Biochemistry, University of Bristol
School of Medical Sciences, University Walk, Bristol, BS8 1TD (UK)

Supporting information for this article is available on the WWW under http://www.chembiochem.org or from the author.

fatty acid or polyketide ACP. In this work we report the high resolution NMR structures of *Streptomyces coelicolor* actinorhodin (act) apo- and holo-ACP. Both models are of high quality and reveal a subtle but distinctive conformational change between the two forms. Conversion to the holo form creates new intramolecular interactions between the protein and the 4′-PP side chain that could partially drive this rearrangement. We show that the act apo-ACP has higher affinity for ACPS than the holo-form and suggest an alternative mechanism for dissociation of the ACPS–holo-ACP complex.

Results and Discussion

Apo-ACP data and structural quality

With the benefit of three-dimensional NMR spectroscopy data and more up-to-date structural calculation methods, it was possible to determine a greatly improved structure for act apo-ACP. Our previous work used 699 NOE distance restraints and 94 angle restraints to calculate an ensemble of 24 structures (PDB ID: 1af8) and an average, refined structure (PDB ID: 2af8; Figure 1 A).[11] The updated structure used 2826 NOE distance restraints, 64 ϕ/ψ restraints from TALOS[12] and 50 ϕ restraints from ^3J measurements. The NOE distance restraints were the result of 3566 NOE peaks automatically assigned by the ARIA algorithm,[13] and yielded 1984 unambiguous and 842 ambiguous restraints (Table 1). Of these, 945 were intraresidue, 656 were sequential, 435 were short-range, 816 were long-range, and several ambiguous restraints were classed as both sequential *and* long-range. A total of 100 structures were calculated, and the best 20 were selected according to total energy. These were then subjected to a short (9.4 ps) refinement in water to yield the final bundle of structures (Figure 1 B). There were no NOE restraint violations greater than 0.3 Å, a total of one TALOS violation greater than 5° and an average of two $^3J_{HN}$ restraint violations greater than 1 Hz per structure.[14] The single TALOS restraint violation is for the ψ angle of Thr3 in the flexible N-terminal part of the protein. The ensemble is well defined, with a root mean square deviation (RMSD) to average coordinates for well-ordered backbone atoms of 0.37 Å[15] and 0.79 Å over all backbone atoms. This compares favourably to 1.01 Å and 1.47 Å, respectively, which

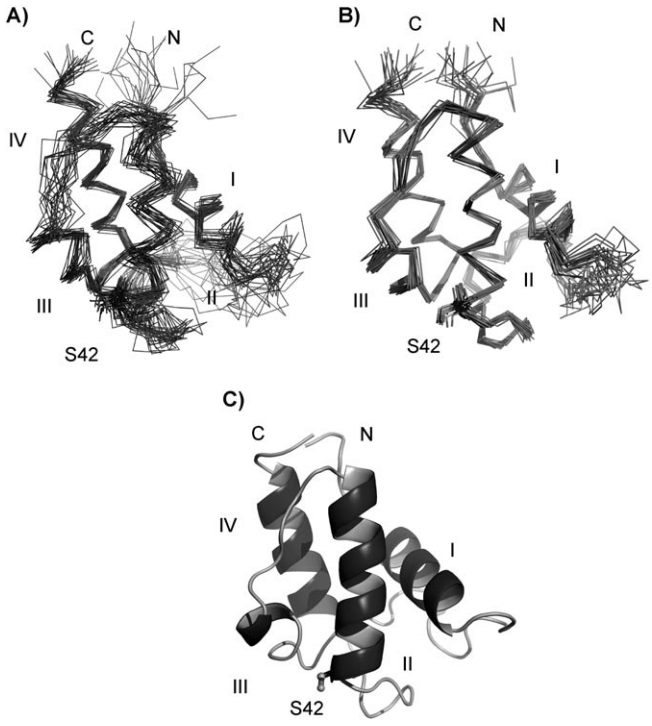

Figure 1. A) Original ensemble of 24 apo-ACP structures (PDB ID: 1af8). B) Updated ensemble of 20 apo-ACP structures. C) Cartoon view of the closest-to-average structure from the new ensemble. N and C termini and helices are labelled.

Table 1. Summary of restraint data and structural quality of NMR models for 1af8 and the new apo- and holo-ACP structures.

	1af8	apo	holo		1af8	apo	holo
Number of peaks				**RMSD to restraints**			
^{13}C NOESY	–	2627	2277	bonds [Å]	0.010	0.014	0.013
^{15}N NOESY	–	939	896	angles [°]	1.4	1.2	1.2
F1,F2 filtered NOESY	–	–	20	NOE [Å]	0.018	0.009	0.006
% not used	–	21	24	TALOS [°]	–	0.16	0.17
Number of restraints				**Precision (RMSD to mean, Å)**			
total	793	2940	2496	all residues (BB atoms)	1.47	0.79	0.81
unambiguous	–	1984	1722	well-ordered residues (BB)	–	0.37	0.42
ambiguous	–	842	715	Ramachandran plot regions [%]			
intraresidue	240	945	946	most favoured	70.6	91.1	88.8
sequential	235	656	531	additionally allowed	25.4	7.8	10.1
short-range	131	439	325	generously allowed	2.9	0.5	0.8
long-range	93	816	635	disallowed	1.1	0.7	0.3
TALOS ϕ/ψ	–	64	59	**WHATCHECK *Z* scores**			
^3J ϕ	94*	50	–	2nd generation packing quality	−2.9	−0.6	−1.2
Violations per structure				**Ramachandran plot appearance**	−6.0	−1.6	−2.5
NOE > 0.3 Å	0	0	0	χ_1/χ_2 rotamer normality	−6.5	−1.8	−1.4
NOE > 0.1 Å	–	6.2	2.0	backbone conformation	−9.2	−4.6	−4.9
TALOS > 5°	–	0.05	0	**WHATCHECK bumps**			
^3J > 1 Hz	–	2.3	–	per 100 residues	25.8	2.6	2.5

* 1af8 used 63 ϕ, 29 χ_1 and 2 χ_2 angle restraints.

were obtained for ACP structure 2af8.[11] The ACP forms a bundle of four α-helices comprised of residues 7–18 (helix I), 42–56 (helix II), 62–65 (helix III) and 71–83 (helix IV; Figure 1C).[16] Loops 1 and 2 connect helices I to II and II to III, respectively. Overall, the updated structure for apo-ACP is 51% helical compared to 49% in 2af8. Helices II and III, which are less well defined in 2af8, have RMSDs of only 0.39 and 0.52 Å in the new bundle. The N and C termini have high RMSDs (>1.8 Å), which reflects their flexibility and low NOE content, as does the unstructured part of the loop region (loop 1, residues 19–29) between helix I and II.

Although qualitatively similar, the new ensemble is of higher quality, both in terms of agreement with experimental restraints and in terms of standard structure quality indicators. The updated ensemble has nearly 99% of residues within the most favoured and additionally allowed regions of the Ramachandran plot (Table 1). The few that fall in the generously allowed or disallowed regions are mainly part of loop 1 between residues 19–29. These residues were only loosely restrained because they showed few NOEs, did not yield good TALOS dihedral angle predictions and had averaged $^{3}J_{HN\alpha}$ coupling constants. Whereas 1af8 ensemble scores poorly with WHATCHECK *Z* scores,[17] those for the updated structure of apo-ACP are much improved (−4.6) and compare favourably with values for the RECOORD database of refined NMR structures.[18,19] A like-for-like comparison to the RECOORD database of refined NMR structures gives a backbone *Z* score of only −0.3.

Chemical-shift mapping

The ^{1}H,^{15}N heteronuclear single quantum coherence (HSQC) spectra for apo- and holo-ACP are compared in Figure 2A–C. The weighted average chemical shift difference $\Delta\delta_{av}$ (ppm) values for apo- versus holo-ACP are plotted against residue number in Figure 2D.[20] This analysis showed that 90% of actinorhodin PKS apo- and holo-chemical shifts matched with an average difference of 0.03 ppm. Most peaks therefore superimpose perfectly between the two spectra; this indicates qualitatively that, as seen in previous studies, the overall structure of the protein appears to be the same following addition of the 4′-PP side chain.

This result is in agreement with the finding that 89% of *Escherichia coli* FAS ACP weighted average shifts (^{1}H and ^{15}N) agreed within 0.1 ppm.[21] Many of the remaining 10%, however, differ quite substantially between the two forms with an average difference of 0.21 ppm and a maximum of 0.5 ppm. These residues are concentrated on helix III (Asp62, Val64 and Gly66) and the first half of helix II near the phosphopantetheine attachment site (Asp41, Ser42, Leu43, Leu45, Met46 and Glu47). These match reasonably closely with the most perturbed residues reported on phosphopantetheinylation of *Bacillus subtilis* FAS,[6] *E. coli* FAS[7] and *Mycobacterium tuberculosis* AcpM[8] ACPs. The presence of a single set of ^{1}H–^{15}N correlation

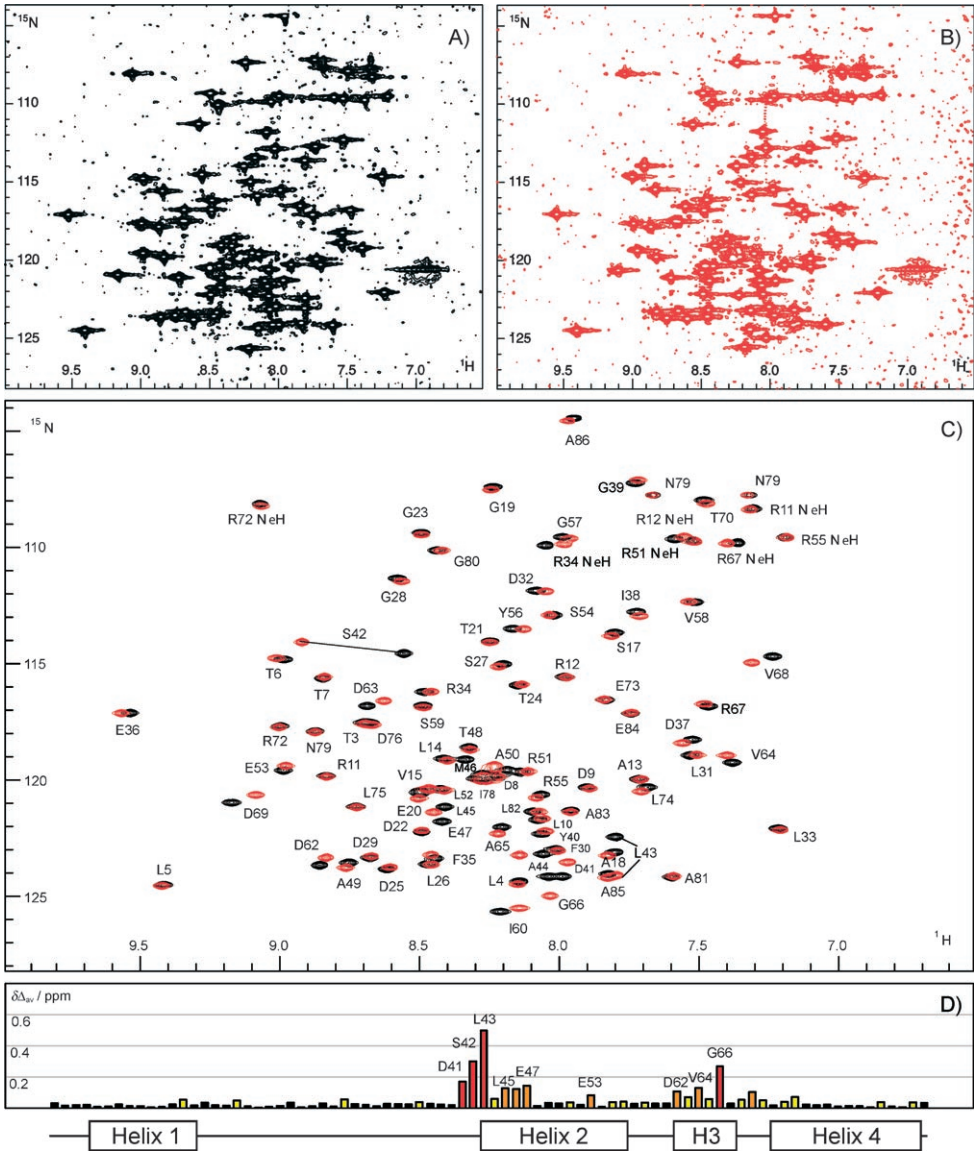

Figure 2. ^{1}H,^{15}N HSQC spectra of apo- (A) and holo-ACP (B), contoured just above the level of noise. C) Superimposed ^{1}H,^{15}N HSQC spectra of apo- (black) and holo-ACP (red). Each peak shows the chemical shift of the nitrogen and proton that make up each amide or amino group. The peaks for all side-chain amides, plus those for Ala86 and Gly66 appear at aliased chemical shifts in the ^{15}N dimension. D) Chemical-shift perturbations ($\Delta\delta_{av}$) are plotted against residue number below the main spectrum. Residues with $\Delta\delta_{av} \geq 0.04$, 0.08 and 0.16 ppm are coloured yellow, orange and red, respectively.

peaks suggests the presence of a single conformer for both the apo and holo forms of act apo-ACP. In contrast, the holo form of frenolicin (fren) ACP from *Streptomyces roseofulvus* shows slow exchange on a NMR timescale ($k_{ex} < 1000\ s^{-1}$) for a number of residues in the loop–helix III region.[22] Similarly, slow exchange has been observed in spinach ACP and PfACP. This led to twice as many peaks as expected in the ^{1}H,^{15}N HSQC spectra of spinach ACP and duplication of Val41, Ala60 and Leu61 peaks in PfACP.[10,23] Lastly, self consistency of NOESY datasets demonstrates that intermediate to fast exchange is not present in either forms. Fast conformational rearrangements have been observed in the *E. coli* holo-ACP, requiring several models for correct fitting of the NOE data.[24,25]

Holo-ACP data and structural quality

The structure of holo-ACP was calculated on the basis of 2437 NOE distances and 59 TALOS ϕ/ψ restraints. Of the NOE distance restraints, 946 were intraresidue, 531 were sequential, 325 were short-range and 635 were long-range. In addition to standard ^{13}C- and ^{15}N-edited NOESY spectra, an F1,F2-filtered NOE spectrum was recorded for holo-ACP. This, in combination with the standard data, allowed the definition of 22 intraphosphopantetheine and three protein-to-phosphopantetheine restraints. A total of 100 models were calculated and the 20 with the lowest energy were selected and water refined.

The final ensemble is shown in Figure 3A. There were no NOE violations greater than 0.3 Å, only two NOE violations per structure greater than 0.1 Å and no TALOS violations greater than 5°. The structures were of high quality. Over 98% of residues fell within the most favoured and additionally allowed regions of the Ramachandran plot, and WHATCHECK *Z* scores were favourable (Table 1). The secondary structure of holo-ACP was assigned with DSSP,[16] which shows that it adopts an identical four-helical bundle to that seen for the apo form. The closest to average structure is shown in Figure 3B. Overall, holo-ACP is well defined, with RMSDs to the mean coordinates of 0.42 and 0.81 Å over well-ordered residues and all residues, respectively. In comparison to the apo structure reported here, the first half of the loop that connects helices I and II (residues Gly19–Ser29) is less structured with an RMSD of 2.22 Å. Three restraints from the protein to 4′-PP side chain were identified. These all originated from the methyls of Leu43 and the pantothenate methyls of the cofactor. The remainder of the phosphopantetheine arm adopted an essentially random conformation with an RMSD to mean coordinates of 4.25 Å.

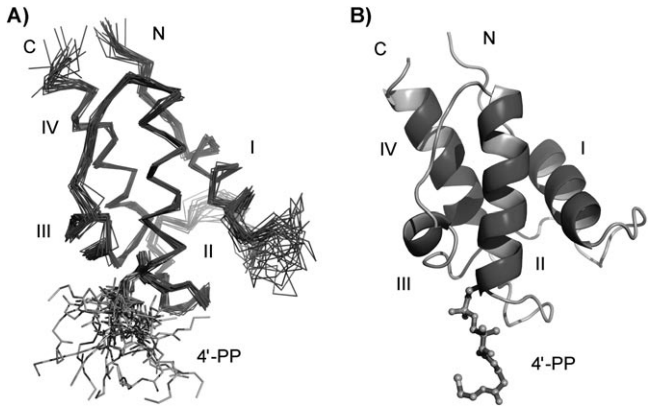

Figure 3. A) Final ensemble of 20 holo-ACP structures. B) Closest-to-average model.

Comparison of apo and holo forms

Both the apo and holo structures are of high quality. The number of restraints used exceeds the number used in other recent ACP solution structures,[6,10,22,26,27] and the structures show better Ramachandran plot profiles (88.8–91.1% in most favoured regions vs. typically 68–83%). A common thread in numerous studies of apo- and holo-ACP is that they are essentially the same, as visual comparison of NOE strips for the two are almost indistinguishable.[6,7,11,21] During peak picking in the run up to the full structure calculations, it was indeed the case that NOE data for the apo and holo forms were notable mainly for their similarities rather than their differences. Apart from small changes adjacent to the site of prosthetic group attachment (Ser42 Oγ), the NOE strips of residues Ser42, Leu43, Ala44 and Leu45 were virtually identical with the exception of the new NOEs identified for the 4′-PP side chain. Superposition of the closest to average holo-ACP model was compared to the equivalent apo-ACP model. Alignment over helices I, II and IV yielded a backbone RMSD of 0.80 Å (Figure 4A) and 0.79, 0.71, 1.42 and 0.98 Å over backbone atoms in helix I, II, III and IV, respectively. The conformation of helix I, the ordered part of loop 1 from residue 30–42 and helix II were very similar, despite the attachment of the phosphopantetheine arm at Ser42. However, a phosphopantetheinylation-induced closure of the helix II–III cleft was visible, with helix III moving towards helix II in holo-ACP. This movement is especially pronounced at the N terminus of helix III. The somewhat raised RMSD for helix IV results from a slight rotation in its orientation relative to the apo form, with the N terminus moving towards helix I, and the C terminus moving away from helix II.

Changes in helix II have been previously ascribed to a combination of the presence of the 4′-PP side chain attached to the conserved serine as well as transient interactions with the 4′-PP cofactor.[6–8] However, the assumption that the apo and holo structures were the same means that contributions from conformational change would not have been taken into account. Our observations clearly confirm that Asp41 and Ser42 do not show a quantifiable structural change, and that any chemical-shift perturbations observed are due to the presence of the 4′-PP cofactor.

Leu43 shows the largest chemical-shift change (Figure 2D), a proportion of which is due to the presence of the 4′-PP chain. In addition, Leu43 shows a direct observable interaction through rotation of the hydrophobic side chain and packing against the hydrophobic portion of the cofactor (Figure 4B and C). This conformational change must also contribute to the observed chemical-shift perturbations. The average χ_1 angles for Leu43 were $-173 \pm 6°$ in apo-, and $-72 \pm 23°$ in holo-ACP. The high standard deviation for the holo-ACP angle

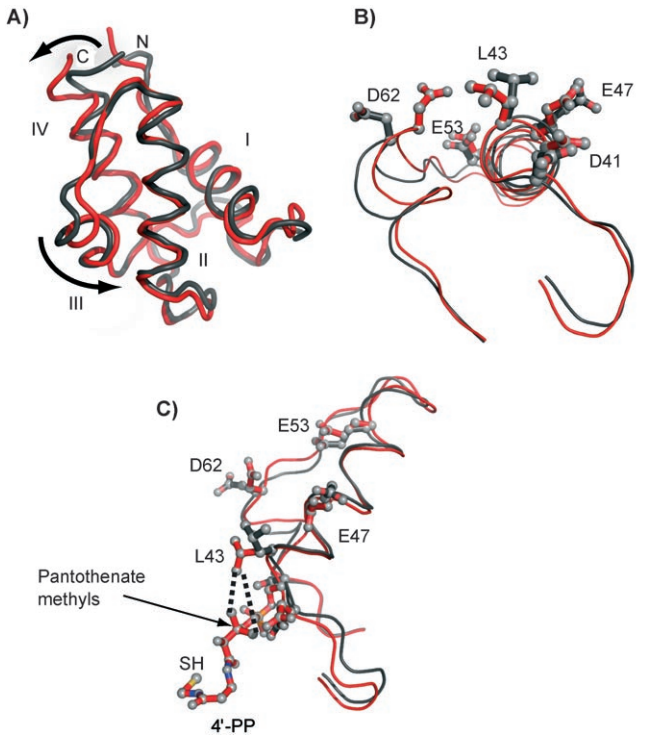

Figure 4. A) Ribbon view from two angles showing the superimposed average structures for the apo- (black) and holo-ACP (red), aligned over helices I, II and IV; B) and C) detailed view showing the relative orientations of Asp41, Leu43, Glu47, Glu53 and Asp62 in the two structures.

was due to a single structure, measured at -165°. Without this outlier, the holo-ACP average becomes $-67\pm8^{\circ}$. As this is the only directly observable interaction with the 4′-PP side chain, it might contribute in part to the changes in loop 2 and helix III. An interaction between the leucine equivalent in PfACP and the cofactor has previously been observed, but its significance to the holo form was lost because no comparison with the apo form was made.[10] However, in the latter case the presence of a minor form with an additional interaction with the equivalent to Met46 (Val41) appears to cause a similar structural change in the helix II–loop–helix III region.

The remaining act helix II residues Leu45, Met46, Glu47 and Glu53 showed small chemical shifts (Figures 2D and 4B). Leu45 is largely buried (relative accessible surface area (ASA) of 5.4) and it is unlikely that contact with the mobile, solvent exposed prosthetic group is responsible for its chemical-shift difference. The observed movement of the loop that connects helix II and III and the movement of helix III towards helix II is a more likely source of perturbation. The rearrangement of helix III is responsible for the observed apo-to-holo chemical shift differences for Asp62, Val64, Gly66. As shown in Figure 4B and C, the whole of Asp62 swings towards helix II and folds across the cleft. Val64 shows a small rearrangement but is partially buried at the interface between helix II and III, whilst Gly66 has only a 16.9% ASA.

Historically apo- and holo-ACPs have been assumed to be almost identical, which may not be expected given that one form must be recognised and one form released by the ACPS. One other NMR spectroscopy investigation has compared the apo and holo forms of the peptidyl carrier protein (PCP) from the nonribosomal peptide synthetase (NRPS) for tyrocidine A (tyc). This showed three distinct conformers with apparently different functions. The apo form (A) was specifically recognised by the phosphopantetheinyl transferase, Sfp, whereas the holo form (H) was specifically recognised by the thioesterase, SrfTEII. Finally, the most structured intermediate A/H state was common to both apo- and holo-PCP.[28] However, comparison with PKS ACP is difficult as the PCP structures are extremely unusual. Analysis by using the RECOORD database reveals, for example, that the tyc-PCP A state has χ_1/χ_2 rotamer normality and backbone conformation parameters more than five standard deviations outside the average for 500+ RECOORD entries. The quality of our models has allowed us to confidently assign gross and residue-specific conformational changes between apo- and holo-ACP. The helix II loop and helix III move towards helix II; this constricts any hydrophobic cleft between these helices. Although we do not observe slow exchange in the present study, the location of structural changes between act apo- and holo-ACP clearly coincides with mobile regions observed in fren holo-ACP. Mobility in this region is also required to open the fatty acid binding cavity observed in crystal and NMR structures of acyl-bound ACPs, although, interestingly, this involves a movement of helix III in the opposite direction, away from helix II.[29,30]

Affinity of act apo- and holo-ACP for *S. coelicolor* FAS ACPS

Given that structural changes were induced upon conversion from inactive to active forms of the carrier protein, we looked for changes in biochemical properties. Thus, we assayed the binding affinity of act apo- and holo-ACP to *S. coelicolor* FAS ACPS using tryptophan fluorescence to assess the binding affinity to *S. coelicolor* ACPS and electrospray mass spectrometry (ESMS) to analyse the percentage conversion of apo to holo. As expected, fluorescence quenching showed that apo-ACP had a higher affinity for ACPS. Conversion to the holo form, which was complete in two hours, led to a twofold drop in binding affinity (Figure 5A, Table 2). The K_d of apo-ACP agrees well with the upper limit of 1 μM determined for the K_M of the *E. coli* ACPS.[31]

Comparison with holo-ACP in the *B. subtilis* crystal structure

To understand the difference in the ACPS binding affinities of act apo- and holo-ACP, we compared our results to the *B. subtilis* ACP and ACPS NMR and crystal structures.[3,6] NMR spectroscopy data of the uncomplexed apo- and holo-protein were described as "essentially the same", based on a visual interpretation of NOEs, but a full apo structure was not reported. Interestingly, Leu37 and Asp56 in *B. subtilis* ACP (equivalent to Leu43 and Asp62 in act ACP) also showed large chemical-shift differences between free apo and holo forms, and were noted in the crystal structure for their importance at the binding interface. The chemical-shift differences appeared to translate to structural differences between ACP's bound and free holo

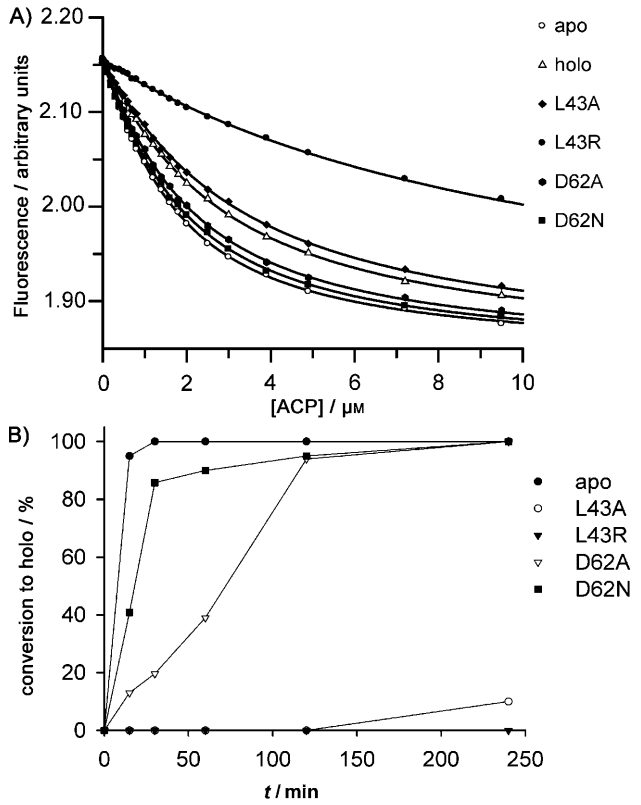

Figure 5. Fluorescence quenching of apo-, holo-, L43A, L43R, D62A and D62N ACPs upon binding of *S. coelicolor* ACPS. B) Percentage conversion to the holo form over a 4 h time-course; conversion was assayed by using ESMS.

Table 2. Derived K_d values for the interaction of act ACP with ACPS and efficiency of phosphopantetheine transfer.

ACP[a]	K_d [μM]	Activity [%][b]
apo	1.1 ± 0.1	100
holo	2.1 ± 0.1	–
L43A	2.7 ± 0.1	15
L43R	10.2 ± 0.2	0
D62A	1.6 ± 0.1	86
D62N	1.3 ± 0.1	20

[a] ACP mutant used in the assay; [b] % conversion to holo after 30 min.

forms. Comparison of the two gave a RMSD of 1.57 Å for backbone atoms in regions of defined secondary structure.

Figure 6A shows the complex of *B. subtilis* ACP with ACPS. Leu37 is clearly sequestered in a hydrophobic pocket formed by residues Ile15, Met18, Phe25 and Phe54. Sequence alignment of FAS ACPS from *S. coelicolor* and *B. subtilis* shows the presence of equivalent hydrophobic residues Phe16 (Ile15), Ala19 (Met18), Leu26 (Phe25), Phe53 (Phe54). Superposition of act apo-ACP residues 7–18 and 35–75 with bound and free *B. subtilis* holo-ACP (residues 4–15 and 29–69) yields an RMSD of 1.70 Å and 2.2 Å, respectively. The act apo-ACP structure is therefore more similar to the ACPS bound form of *B. subtilis* ACP. When this alignment was used to superimpose the act apo-ACP Cα atoms onto *B. subtilis* ACP in the ACP–ACPS complex, the Leu37 homologue, Leu43, is positioned ideally for

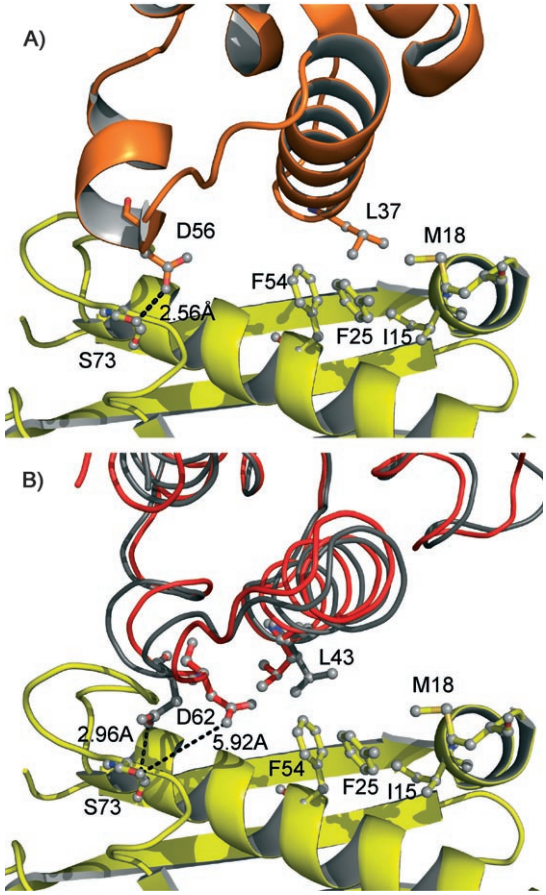

Figure 6. A) *B. subtilis* holo-ACP–ACPS cocrystal structure, with ACP (orange) and ACPS (yellow). The hydrogen bonding partner of ACP residue Asp56 is shown, as is the hydrophobic pocket that binds Leu37. B) Superimposed structures of actinorhodin apo- (black) and holo-ACP (red) aligned to the *B. subtilis* ACP over Cα atoms. The homologous residues Leu43 and Asp62 in apo-ACP are well-placed to enter productive bonding with ACPS, whereas those in holo-ACP are not.

binding in the hydrophobic pocket. In contrast, Leu43 on act holo-ACP is held away from the binding pocket, and instead forms interactions with the methyl groups of the phosphopantetheine side chain. This could suggest that once modified to the holo form, the potential for a new intramolecular interaction with the 4′-PP chain might compete with the interaction of this residue with the hydrophobic pocket and provide energetic compensation for dissociation of the complex.

Although often not highlighted, the hydrogen bonding interaction of the equivalents to act ACP Asp62 are clearly important for efficient ACPS function in several systems.[4,5,32] In the *B. subtilis* ACPS–ACP complex, Asp56 forms a hydrogen bond to the side chain OH of ACPS Ser73. Asp62 in act apo-ACP is within hydrogen bonding distance of Ser73 when modelled onto the *B. subtilis* complex (2.96 Å from Asp62 Oδ1 to Ser73 Oγ). Rotation of helix III in holo-ACP would result in Asp62 to shift away from this interaction and give a final Asp62 Oδ1 to Ser73 Oγ distance of 5.92 Å, which is clearly beyond hydrogen bonding range. However, Ser73, which lies in a loop that connects α-helix 4 to β-strand 2, is not conserved and is replaced by Leu70 in the *S. coelicolor* ACPS.

Clearly no hydrogen bonding interaction is possible in this case, although it is possible that Thr72 might act as a substitute for Ser73.

Mutation of Leu43 and Asp62 and its effect on *S. coelicolor* FAS ACPS binding and phosphopantetheine transfer

In order to assess the influence of Leu43 and Asp62 for binding and ACPS activity, site-directed mutagenesis was used to generate four single-point mutations of act ACP: L43A, L43R, D62A and D62N. The effects of each mutation were then compared to the results previously obtained for the apo and holo forms (Figure 5, Table 2). Replacement of hydrophobic Leu43 with alanine produced a binding profile very similar to that of holo-ACP, with a twofold reduction in binding. Modification of this mutant to the holo form correlated well with the fall in affinity, with only 15% conversion compared to the wild type. The most significant effect was observed with L43R, which had tenfold weaker binding and was completely inactive in the phosphopantetheine transfer assay. Finally, the mutations D62A and D62N had less influence, but nonetheless both exhibited a ~40 and 20% drop in binding affinity, respectively. Over a 4 h incubation time-course both D62A and D62N mutant carrier proteins achieved 100% conversion to the holo form (Figure 5B), though the rates of phosphopantetheinylation reflected their differential binding to ACPS. The D62N mutant, which exhibited only a 20% reduction in binding affinity, was completely activated within 60 min (compared to 15 min for the wild-type apo-protein), while the D62A mutant achieved the same levels of holo modification only after 2 h of incubation with the *S. coelicolor* ACPS. Finally, to check for possible gross structural perturbations of the act ACP tertiary structure, a ^{15}N labelled sample of each mutant ACP was prepared. A $^{1}H,^{15}N$ HSQC spectrum was recorded for each protein and compared with the apo form (Figure S1 in the Supporting Information). The spectra all superimpose well. For L43A and L43R the major chemical-shift perturbations are for residues in helix II. L43R shows fewer overall changes than L43A but shows the largest reduction in ACPS binding and activity. For D62A and D62N the perturbations lie in helix III and loop 2. There is no evidence for a major change in tertiary fold, but minor changes around the site of point mutations cannot be ruled out.

The role of the hydrophobe in the DSL motif

Both Leu43 and Asp62 clearly modulate binding of apo- and holo-ACP to the *S. coelicolor* group I ACPS, and mutation of Leu43 arguably has the strongest effect. Leu43 forms part of the D/E/H-S-L/I/V/M motif that is highly conserved in FAS, type II PKS ACPs and NRPS PCPs.[1,27] Several structural studies have highlighted its importance in protein recognition.[34] The *B. subtilis* ACPS used in the cocrystallisation studies is a member of the group I trimeric phosphopantetheine transferases (PPT), which possess an ACP binding interface between each domain. The ACP contributes predominantly specific electrostatic interactions from the negatively charged residues on the recognition helix II and the aspartate of the DSL motif of the ACP.[3,35,36] Conservation of these charged residues in type II bacterial and polyketide ACPs allows ACPS to modify both forms, with an efficiency that broadly correlates to overall negative charge. The hydrophobic interaction highlighted between Leu43 and the ACPS pocket is one of only two hydrophobic contacts identified in the complex. However, the hydrophobic pocket into which Leu43 (or equivalents) would bind is highly conserved. Sequence alignments of 185 ACPS sequences revealed almost complete conservation of hydrophobicity in this pocket. (Three exceptions showed a single polar substitution at only one of these positions).

Although the *S. coelicolor* type II polyketide ACP can be modified by the ACPS group I PPT, this class is thought to be primarily utilised by type II bacterial FASs. Type I FASs and PKSs, NRPSs and the majority of type II PKSs utilise more promiscuous group II PPTs.[37–40] Three-dimensional structures of uncomplexed *B. subtilis* nonribosomal peptide surfactin synthetase (Sfp) PPT and the human type I PPT in complex with the type I FAS ACP have been solved.[37,39] These proteins show a different fold to group I PPTs and comprise a covalently linked didomain rather than a trimeric assembly. Nonetheless, the ACP binding interface topology formed between the subunits is similar. Mutational studies have shown that Sfp employs an alternate electrostatic complementarity for recognition of peptidyl carrier proteins, but still binds helix II of the PCP or ACP.[41] However a structure of a Sfp–PCP complex has not been reported. The human type II PPT–type I FAS ACP complex shows the interaction was derived mainly from hydrophobic contacts rather than any specific electrostatic complementarity. The Leu43 analogue, Leu2157, in the human type I FAS ACP, is conserved in the mammalian type I FAS ACPs and alongside two further hydrophobes, Met2158 and Val2160, it interacts with a hydrophobic patch on PPT. Mutation of all three ACP hydrophobes reduces the K_m for PPT by three orders of magnitude.

The importance of several polar and hydrophobic residues has also been tested with the FAS ACP from *E. coli* (AcpP) by using in vitro modification of the mutant AcpP with ACPS and in vivo complementation of *E. coli* strains with fatal temperature sensitive mutations in the AcpP gene.[5] Both L37C and D56C (Leu43 and Asp62 analogues) could be modified in vitro by using ACPS but were unable to complement the null AcpP mutant and restore growth. Therefore, although not critical for ACPS binding, the lack of complementation could indicate that these residues influence binding with other downstream proteins of the fatty acid pathway.

Conclusions

We have generated two high quality structures of apo- and holo-ACP from the same polyketide synthase and shown that there are identifiable differences between them. The principle differences comprise movement of helix III towards helix II and conformational switch of a key residue, Leu43. Comparison with a known ACP–ACPS crystal structure suggests that in the apo form Leu43 is able to interact with a conserved hydrophobic patch on the surface of ACPS, whereas this interaction is

compensated for internally in the holo form by taking advantage of new interactions made possible with the 4′-PP chain. Accordingly mutation of this residue modulates binding to ACPS. On the basis of these observations it is also possible to extend the description of current the ACP–ACPS binding and dissociation mechanism. We have shown that the conformation of apo-ACP might be similar to the reported ACPS bound form and has a higher affinity for ACPS than the holo form. This conformation is also optimised for transfer of the 4′-PP side chain.[3] Once conversion has taken place, dissociation of the ACP–ACPS complex would be initiated by the bound structure of holo-ACP, relaxing to its free conformation.[6]

Experimental Section

Protein preparation: The C17S mutant of act ACP was utilized in all of the NMR studies and in vitro assays, as it has been shown that WT act holo-ACP can form an intramolecular disulphide bridge between the phosphopantetheine thiol and the thiol group of C17.[42] Apo-acyl carrier protein was isotopically ^{15}N, ^{13}C labelled and purified as previously described.[11,43] The addition of the phosphopantetheine portion of the coenzyme A onto ^{15}N, ^{13}C apo-ACP was catalysed by *S. coelicolor* ACPS.[2,44,45] Reactions were repeated on a 500 μL scale and monitored by ESMS. Briefly, ACPS (5 μL, 100 μM solution in the same buffer) and coenzyme A (10 μL, 50 mM solution in D_2O) were added to a solution of apo-ACP (1 mg mL^{-1}) in Tris buffer (485 μL, 50 mM, pH 8.8) containing $MgCl_2$ (10 mM). The reaction was incubated at 30 °C for 1 h with shaking. Twenty reactions were carried out simultaneously. The combined reactions were then concentrated and buffer exchanged into potassium phosphate buffer (20 mM, pH 5.5) by using two Centricon YM-3 devices (2 mL, Millipore). At least three rounds of 5x dilution were performed for the buffer exchange such that the original buffer was diluted to <1% of its starting concentration. The final protein concentration was ~1.7 mM. For holo-ACP, the potassium phosphate buffer was supplemented with tris(2-carboxyethyl)phosphine hydrochloride (TCEP.HCl, 5 mM), care was taken to readjust the pH of the buffer after addition of the TCEP. Electrospray mass spectrometry (ESMS) was performed by using a Fisons Instruments VG Quattro triple quadrupole mass spectrometer as described previously.[46,47]

Protein NMR spectroscopy experiments: Samples consisted of apo- or holo-ACP (2 mM), NaN_3 (1 mM), K_2HPO_4 (20 mM) in D_2O/H_2O (5:95, 600 μL, pH 5.5). All protein NMR spectroscopy experiments were acquired at 25 °C by using a Varian INOVA 600 spectrometer with the BioPack collection of pulse sequences. NMR spectroscopy data were processed by using NMRPipe[48] and analysed by using CCP NMR Analysis version 1.0. The holo PDB file containing the serine modified with the 4′-PP group was created by using the Dundee PRODRG server[49] and imported into CCP NMR Analysis by using CCP NMR Format Converter.[50]

NMR data and analysis: Standard triple resonance experiments were acquired for sequential and side-chain assignment. Structural restraints were derived from a $^{13}C/^{15}N$ NOESY-HSQC.[51] HNHA spectral data for the experimental calculation of ^3J derived ϕ angle restraints was also collected. The F1,F2-filtered TOCSY and NOESY experiments were used to facilitate assignment of side-chain resonances.[52] All structure calculations were carried out using the Ambiguous Restraints for Iterative Assignment of NOEs (ARIA) protocol Version 1.2,[13] which includes an algorithm that attempts to correct for the effects of spin diffusion.[53] Torsion Angle Likelihood Obtained from Shift and sequence similarity (TALOS)[12] was used to predict ϕ and ψ dihedral angle restraints.

Quantitative perturbations in $^1H,^{15}N$ HSQC spectra were calculated as weighted average chemical-shift differences according to the method of Pellecchia et al.[20] by using Equation (1):

$$\Delta\delta_{av} = \{1/2[(\Delta H)^2 + 0.2(\Delta N)^2]\}^{1/2} \quad (1)$$

where ΔH and ΔN are the differences in proton and nitrogen chemical shift, respectively, between the species being compared. The value of ΔH is more strongly weighted to reflect the smaller range over which it varies.

Structure calculation protocol: For structure calculations involving holo-ACP, topology files were created that contained a series of modified amino acids based on serine. They were derived by analogy to existing homologous fragments in the CHARM22 all-atom force field[54] or, where no appropriate surrogate was available, by quantum mechanical calculations on model compounds at the B3LYP/6-31+G(d) level. Initially, structure calculation runs contained eight iterations of 20 structures each, and the best seven structures in each iteration (sorted according to total energy) were used for analysis and assignment. The number of dynamics steps was increased over default values to 20000 and 16000 for the first and second cooling stages, respectively.[55] After each run, violated restraints were checked, and those that arose from noise peaks or incorrect assignments were removed/reassigned. Final ensembles of 100 structures were calculated from calibrated restraint tables. The 20 best structures (sorted according to total energy) were selected for water refinement. Water refined structures were calculated by using the slightly modified refinement script applied to the RECOORD database.[18,19] PROCHECK[56] and WHATCHECK,[17] and quality indicators were compared to the average values for the RECOORD database of protein NMR structures. The solvent accessible surface areas (ASA) of residues in the actinorhodin apo-ACP were compared to 'random-coil' values in a Gly-X-Gly peptide by using the program Get Area 1.1.[57–59] The ratio was expressed as a percentage; residues for which the relative ASA exceeded 50% were considered solvent exposed, whilst those with relative ASA below 20% were considered buried.

The ensemble of 20 NMR structures of act apo-ACP has been deposited with the Brookhaven protein database (PDB ID: 2k0y) and NMR chemical shifts have been deposited with BioMagResBank (accession code: 15659). The ensemble of 20 NMR structures of act holo-ACP has been deposited with the Brookhaven protein database (PDB ID: 2k0x) and NMR chemical shifts have been deposited with BioMagResBank (accession code: 15658).

Analysis of AcpS–ACP interaction by site-directed mutagenesis: *S. coelicolor* act PKS ACP mutants L43A, L43R, D62A and D62N were generated by using the Stratagene QuikChange protocol. The ability of the mutants to act as substrates for *S. coelicolor* holo-ACP synthase in vitro was assayed by incubating apo-ACP (100 μM) and *S. coelicolor* ACPS (2 μM) with coenzyme A in Tris buffer (50 mM, pH 8.8) containing DTT (5 mM) and $MgCl_2$ (10 mM). Assays were quenched after 2 h, and the degree of phosphopantetheinylation was determined by electrospray mass spectrometry.

The affinity of ACPS for apo-, holo- and mutant ACPs was determined by monitoring the change in ACPS intrinsic fluorescence upon titration with ACP. Fluorescence emission was excited at 295 nm and recorded over 320–360 nm by using a slit width of 0.75 μm, and integrated over one second. ACPS (1 μM, 2 mL) was titrated with holo-, apo- and each mutant ACP at 25 °C in Tris

buffer (50 mM, pH 8.8) containing DTT (5 mM) and $MgCl_2$ (10 mM). Plotting the change in fluorescence at the ACPS fluorescence maximum, 337 nm, with increasing ACP concentration (up to 33 μM) allowed the dissociation constant, K_d, for the complex to be determined.

Acknowledgements

This work was supported by the BBSRC (grant No. 7/B20055 and BB/F014570/1) and the HEFCE (equipment grant to the University of Bristol, SRIF-2).

Keywords: bioorganic chemistry · biosynthesis · NMR spectroscopy · polyketides · protein structures

[1] D. M. Byers, H. S. Gong, *Biochem. Cell Biol.* **2007**, *85*, 649–662.
[2] R. H. Lambalot, A. M. Gehring, R. S. Flugel, P. Zuber, M. LaCelle, M. A. Marahiel, R. Reid, C. Khosla, C. T. Walsh, *Chem. Biol.* **1996**, *3*, 923–936.
[3] K. D. Parris, L. Lin, A. Tam, R. Mathew, J. Hixon, M. Stahl, C. C. Fritz, J. Seehra, W. S. Somers, *Structure* **2000**, *8*, 883–895.
[4] L. M. Worsham, L. Earls, C. Jolly, K. G. Langston, M. S. Trent, M. L. Ernst-Fonberg, *Biochemistry* **2003**, *42*, 167–176.
[5] N. R. De Lay, J. E. Cronan, *J. Biol. Chem.* **2007**, *282*, 20319–20328.
[6] G. Y. Xu, A. Tam, L. Lin, J. Hixon, C. C. Fritz, R. Powers, *Structure* **2001**, *9*, 277–287.
[7] Y. Kim, E. L. Kovrigin, Z. M. Eletr, *Biochem. Biophys. Res. Commun.* **2006**, *341*, 776–783.
[8] H. C. Wong, G. H. Liu, Y. M. Zhang, C. O. Rock, J. Zheng, *J. Biol. Chem.* **2002**, *277*, 15874–15880.
[9] Q. Li, C. Khosla, J. D. Puglisi, C. W. Liu, *Biochemistry* **2003**, *42*, 4648–4657.
[10] A. K. Sharma, S. K. Sharma, A. Surolia, N. Surolia, S. P. Sarma, *Biochemistry* **2006**, *45*, 6904–6916.
[11] M. P. Crump, J. Crosby, C. E. Dempsey, J. A. Parkinson, M. Murray, D. A. Hopwood, T. J. Simpson, *Biochemistry* **1997**, *36*, 6000–6008.
[12] G. Cornilescu, F. Delaglio, A. Bax, *J. Biomol. NMR* **1999**, *13*, 289–302.
[13] M. Nilges, M. J. Macias, S. I. O'Donoghue, H. Oschkinat, *J. Mol. Biol.* **1997**, *269*, 408–422.
[14] D. S. Garrett, J. Kuszewski, T. J. Hancock, P. J. Lodi, G. W. Vuister, A. M. Gronenborn, G. M. Clore, *J. Magn. Reson. B* **1994**, *104*, 99–103.
[15] M. Nilges, G. M. Clore, A. M. Gronenborn, *FEBS Lett.* **1987**, *219*, 11–16.
[16] W. Kabsch, C. Sander, *Biopolymers* **1983**, *22*, 2577–2637.
[17] R. W. Hooft, G. Vriend, C. Sander, E. E. Abola, *Nature* **1996**, *381*, 272.
[18] A. J. Nederveen, J. F. Doreleijers, W. Vranken, Z. Miller, C. A. E. M. Spronk, S. B. Nabuurs, P. Güntert, M. Livny, J. L. Markley, M. Nilges, E. L. Ulrich, R. Kaptein, A. M. J. J. Bonvin, *Proteins Struct. Funct. Bioinf.* **2005**, *59*, 662–672.
[19] J. P. Linge, M. A. Williams, C. A. E. M. Spronk, A. M. J. J. Bonvin, M. Nilges, *Proteins* **2003**, *50*, 496–506.
[20] M. Pellecchia, P. Sebbel, U. Hermanns, K. Wüthrich, R. Glockshuber, *Nat. Struct. Biol.* **1999**, *6*, 336–339.
[21] M. Andrec, R. B. Hill, J. H. Prestegard, *Protein Sci.* **1995**, *4*, 983–993.
[22] Q. Li, C. Khosla, J. D. Puglisi, C. W. Liu, *Biochemistry* **2003**, *42*, 4648–4657.
[23] G. A. Zornetzer, R. D. White, J. L. Markley, B. G. Fox, *Protein Expression Purif.* **2006**, *46*, 446–455.
[24] T. A. Holak, S. K. Kearsley, Y. Kim, J. H. Prestegard, *Biochemistry* **1988**, *27*, 6135–6142.
[25] T. A. Holak, M. Nilges, J. H. Prestegard, A. M. Gronenborn, G. M. Clore, *Eur. J. Biochem.* **1988**, *175*, 9–15.
[26] V. Y. Alekseyev, C. W. Liu, D. E. Cane, J. D. Puglisi, C. Khosla, *Protein Sci.* **2007**, *16*, 2093–2107.
[27] E. Ploskon, C. J. Arthur, S. E. Evans, C. Williams, J. Crosby, T. J. Simpson, M. P. Crump, *J. Biol. Chem.* **2008**, *283*, 518–528.
[28] A. Koglin, M. R. Mofid, F. Löhr, B. Schäfer, V. V. Rogov, M. M. Blum, T. Mittag, M. A. Marahiel, F. Bernhard, V. Dötsch, *Science* **2006**, *312*, 273–276.
[29] A. Roujeinikova, C. Baldock, W. J. Simon, J. Gilroy, P. J. Baker, A. R. Stuitje, D. W. Rice, A. R. Slabas, J. B. Rafferty, *Structure* **2002**, *10*, 825–835.
[30] A. Roujeinikova, W. J. Simon, J. Gilroy, D. W. Rice, J. B. Rafferty, A. R. Slabas, *J. Mol. Biol.* **2007**, *365*, 135–145.
[31] R. H. Lambalot, C. T. Walsh, *J. Biol. Chem.* **1995**, *270*, 24658–24661.
[32] H. Gong, A. Murphy, C. R. McMaster, D. M. Byers, *J. Biol. Chem.* **2007**, *282*, 4494–4503.
[33] M. A. Johnson, W. Peti, T. Herrmann, I. A. Wilson, K. Wüthrich, *Protein Sci.* **2006**, *15*, 1030–1041.
[34] H. D. Mootz, R. Finking, M. A. Marahiel, *J. Biol. Chem.* **2001**, *276*, 37289–37298.
[35] N. Y. Chirgadze, S. L. Briggs, K. A. McAllister, A. S. Fischl, G. Zhao, *EMBO J.* **2000**, *19*, 5281–5287.
[36] Y. M. Zhang, B. N. Wu, J. Zheng, C. O. Rock, *J. Biol. Chem.* **2003**, *278*, 52935–52943.
[37] K. Reuter, M. R. Mofid, M. A. Marahiel, R. Ficner, *EMBO J.* **1999**, *18*, 6823–6831.
[38] M. R. Mofid, R. Finking, L. O. Essen, M. A. Marahiel, *Biochemistry* **2004**, *43*, 4128–4136.
[39] G. Bunkoczi, S. Pasta, A. Joshi, X. Q. Wu, K. L. Kavanagh, S. Smith, U. Oppermann, *Chem. Biol.* **2007**, *14*, 1243–1253.
[40] K. J. Weissman, H. Hong, M. Oliynyk, A. P. Siskos, P. F. Leadlay, *ChemBioChem* **2004**, *5*, 116–125.
[41] R. Finking, M. R. Mofid, M. A. Marahiel, *Biochemistry* **2004**, *43*, 8946–8956.
[42] J. Crosby, K. J. Byrom, T. S. Hitchman, R. J. Cox, M. P. Crump, I. S. C. Findlow, M. J. Bibb, T. J. Simpson, *FEBS Lett.* **1998**, *433*, 132–138.
[43] S. C. Findlow, C. Winsor, T. J. Simpson, J. Crosby, M. P. Crump, *Biochemistry* **2003**, *42*, 8423–8433.
[44] R. J. Cox, T. S. Hitchman, K. J. Byrom, I. S. C. Findlow, J. A. Tanner, J. Crosby, T. J. Simpson, *FEBS Lett.* **1997**, *405*, 267–272.
[45] R. J. Cox, J. Crosby, O. Daltrop, F. Glod, M. E. Jarzabek, T. P. Nicholson, M. Reed, T. J. Simpson, L. H. Smith, F. Soulas, A. E. Szafranska, J. Westcott, *J. Chem. Soc. Perkin Trans. 1* **2002**, *14*, 1644–1649.
[46] R. L. Winston, M. C. Fitzgerald, *Anal. Biochem.* **1998**, *262*, 83–85.
[47] J. Crosby, D. H. Sherman, M. J. Bibb, W. P. Revill, D. A. Hopwood, T. J. Simpson, *Biochim. Biophys. Acta Protein Struct. Mol. Enzymol.* **1995**, *1251*, 32–42.
[48] F. Delaglio, S. Grzesiek, G. W. Vuister, G. Zhu, J. Pfeifer, A. Bax, *J. Biomol. NMR* **1995**, *6*, 277–293.
[49] A. W. Schüttelkopf, D. M. van Aalten, *Acta Crystallogr. D Biol. Crystallogr.* **2004**, *60*, 1355–1363.
[50] W. F. Vranken, W. Boucher, T. J. Stevens, R. H. Fogh, A. Pajon, M. Llinas, E. L. Ulrich, J. L. Markley, J. Ionides, E. D. Laue, *Proteins Struct. Funct. Bioinf.* **2005**, *59*, 687–696.
[51] S. M. Pascal, D. R. Muhandiram, T. Yamazaki, J. D. Forman-Kay, L. E. Kay, *J. Magn. Reson. Ser. B* **1994**, *103*, 197–201.
[52] R. D. Peterson, C. A. Theimer, H. H. Wu, J. Feigon, *J. Biomol. NMR* **2004**, *28*, 59–67.
[53] J. P. Linge, M. Habeck, W. Rieping, M. Nilges, *J. Magn. Reson.* **2004**, *167*, 334–342.
[54] A. D. MacKerell, D. Bashford, M. Bellott, R. L. Dunbrack, J. D. Evanseck, M. J. Field, S. Fischer, J. Gao, H. Guo, S. Ha, D. Joseph-McCarthy, L. Kuchnir, K. Kuczera, F. T. K. Lau, C. Mattos, S. Michnick, T. Ngo, D. T. Nguyen, B. Prodhom, W. E. Reiher, B. Roux, M. Schlenkrich, J. C. Smith, R. Stote, J. Straub, M. Watanabe, J. Wiórkiewicz-Kuczera, D. Yin, M. Karplus, *J. Phys. Chem. A J. Phys. Chem. B* **1998**, *102*, 3586–3616.
[55] M. Fossi, H. Oschkinat, M. Nilges, L. J. Ball, *J. Magn. Reson.* **2005**, *175*, 92–102.
[56] R. A. Laskowski, M. W. Macarthur, D. S. Moss, J. M. Thornton, *J. Appl. Crystallogr.* **1993**, *26*, 283–291.
[57] B. Lee, F. M. Richards, *J. Mol. Biol.* **1971**, *55*, 379–400.
[58] R. Fraczkiewicz, W. Braun, *J. Comput. Chem.* **1998**, *19*, 319–333.
[59] S. J. Hubbard, S. F. Campbell, J. M. Thornton, *J. Mol. Biol.* **1991**, *220*, 507–530.

Received: March 24, 2008
Published online on September 3, 2008

